Influence of conduction electrons on the magnetism of cobalt grains in a copper matrix studied by density-functional theory

J. A. Gómez and Diana Guenzburger*
Centro Brasileiro de Pesquisas Físicas, Rua Dr. Xavier Sigaud 150, Urca, 22290-180, Rio de Janeiro, RJ, Brazil
(Received 5 September 2000; published 28 February 2001)

Electronic structure calculations in the local spin-density approximation were performed for clusters of 79 atoms embedded in a Cu matrix. The discrete variational method was employed. Cobalt grains of up to 55 atoms surrounded by Cu were considered; the lattice parameter of Cu was used for the calculations. Local magnetic moments and hyperfine fields were obtained for all the clusters. The results show that the local magnetic moments at the Co atom sites have oscillatory behavior with a tendency to increase in the direction of the grain boundaries. The magnitude of the contact contribution to the hyperfine field at the Co atom sites also has oscillatory behavior but with a tendency to decrease from the center to the surface of the grains. This is due to a tendency of alignment of the 4*s* moment with the 3*d* moment. Dipolar contributions to the hyperfine field were also calculated for the cobalt atoms at the boundary of the grains. The highest magnitude of this contribution was 4.2 T, found for the grain with 13 Co atoms. Charge oscillations on Co are observed from the center to the surface.

DOI: 10.1103/PhysRevB.63.134404 PACS number(s): 75.20.Hr, 73.22.−f, 71.15.Mb

I. INTRODUCTION

Since the discovery of giant magnetoresistance (GMR) in granular magnetic systems[1,2] produced by dc sputtering, interest in the research of these materials has increased greatly due to potential applications in magnetic recording, sensors, etc. The system that has been most extensively investigated is Co grains in Cu. Experiments reported show the GMR effect and characterize its structural, magnetic, and transport properties.[3–9] Due to the special role played by the unfilled *d* bands in the transport properties of transition metals,[10] electronic structure calculations are useful for the understanding of local magnetism in these systems. From the experimental point of view, techniques that measure the magnetic hyperfine field in transition metals are Mössbauer spectroscopy and nuclear magnetic resonance (NMR). For the granular Co–Cu system, magnetic hyperfine fields have been measured by NMR, with samples prepared by mechanical alloying[11] and melt spinning.[12,13] Another useful technique for studying the local magnetism in metals is x-ray magnetic circular dichroism (XMCD); using ''sum rules'' [14] it is possible to calculate the spin and orbital contributions to the local magnetic moment (LMM). For the Co–Cu system, this technique has been used to measure the magnetic moment mainly in magnetic multilayers of Co on copper substrate.[15–18] To our knowledge, there is only one work reporting measurements of LMM using this technique on clusters of Co embedded in copper.[19]

Only two first-principles electronic structure calculations for grains of cobalt atoms in a copper host are reported in the literature;[20,21] other works address free clusters of cobalt.[22–24] This is due to the fact that band-structure calculations may only be carried out for systems with periodicity, and thus the lack of periodicity introduced by the grains in the host increases the complexity of the theoretical calculations. However, with the use of embedded-cluster methods in real space, it is possible to perform electronic structure calculations for these systems.

Nogueira and Petrilli[20] performed electronic structure calculations for clusters of up to 135 cobalt atoms in a copper matrix, using the real space-linear muffin tin orbital method in the atomic sphere approximation (RSLMTOASA). The authors found that both the local magnetic moment and the magnetic hyperfine field have a tendency to decrease at Co atom sites in the proximity of the interface of the grains. Chuanyun *et al.*[21] performed electronic structure calculations for free clusters of Co and clusters of Co in a Cu matrix of up to 43 Co atoms, employing an embedded-cluster discrete variational method. They obtained an opposite tendency for their calculated LMM, as compared to Ref. 20. They found higher total magnetic moments for the free clusters of Co than for the grains of Co in Cu, with increasing LMM in the direction of the interface of the clusters.

In this work we report first-principles electronic structure calculations, employing the discrete variational method (DVM)[25–27] in the framework of density-functional theory (DFT)[28] and the local spin-density approximation (LSDA), for cobalt clusters of up to 55 atoms in a copper host. We report results for local magnetic moments and magnetic hyperfine fields at the cobalt sites. For the magnetic hyperfine field, we considered the contact (Fermi) contribution for all the cobalt sites. In addition to the contact contribution, at cobalt sites near and at the grain boundaries we considered dipolar contributions.

In Sec. II we briefly describe the theoretical method employed; in Sec. III, we present and discuss the results; and in Sec. IV we summarize our conclusions.

II. THEORETICAL METHOD

The discrete variational method (DVM),[25–27] in the framework of density-functional theory (DFT)[28] and the local spin-density approximation, has been employed for the calculations. A brief summary of the method and details of the calculations will be given here. One seeks the self-consistent solutions of the set of one-electron Kohn–Sham

equations in a three-dimensional grid of points to obtain the eigenvectors, eigenvalues, and Mulliken atomic orbital populations. The local exchange-correlation potential term in the Kohn–Sham Hamiltonian is a functional of the spin-dependent electron density ρ_σ; here we employed the functional of Vosko, Wilks, and Nusair,[29] which is a parametrization of the Ceperley–Alder[30] Monte Carlo simulations. The electron density ρ_σ is defined as the summation of the squared amplitudes of the cluster spin-orbitals $\phi_{i\sigma}$, weighted by their occupation numbers $n_{i\sigma}$, given by Fermi–Dirac statistics. Here we performed spin-polarized calculations, where the electron density has the freedom to be different for each spin σ. The spin density at point $\mathbf{r}$ is defined as $[\rho\uparrow(\mathbf{r}) - \rho\downarrow(\mathbf{r})]$, where the arrow represents the spin of the electron density.

The cluster spin-orbitals are expanded as linear combinations of numerical symmetrized atomic orbitals χ_j (LCAO):

$$\phi_{i\sigma}(\mathbf{r}) = \sum_j \chi_j(\mathbf{r}) C^j_{i\sigma}. \tag{1}$$

The atomic functions of this basis are obtained by self-consistent (SCF) DFT atomic calculations. In the DV method the variational procedure leads to the conventional secular equations which have to be solved self-consistently in a three-dimensional grid:

$$([H]-[S][E])[C]=0, \tag{2}$$

where $[H]$ is the matrix of the Kohn–Sham Hamiltonian, $[C]$ is the matrix of the coefficients in the LCAO, and $[S]$ is the overlap matrix. The criterion for convergence was considered to be a difference $<10^{-3}$ in the charge and spin densities between two successive cycles. The three-dimensional grid was divided in two regions: around each Co atom was placed a sphere of 2.0 a.u. where a precise polynomial integration was performed over a regular grid; outside these spheres a pseudorandom (diophantine)[31,32] scheme was employed to generate points. The number of points used in the calculations depends on the number of Co atoms in the cluster: 5000 points were used inside the sphere of each Co atom and ~400 diophatine points outside; around each Cu atom ~1600 points were used, all diophantine.

A Mulliken-type population analysis to obtain atomic orbital occupations[33] was performed, based on the coefficients of the LCAO expansion, in which the overlap population is distributed proportional to the coefficient of the atom in the cluster spin orbital. To improve the numerical atomic basis set, we employed the atomic orbital occupations resulting from several iterations. This atomic configuration is used to generate new atomic basis functions, more adequate for the cluster environment, by atomic SCF calculations. This procedure is repeated until the atomic configuration obtained is approximately equal to that in the basis. The valence orbitals considered in the variational approach were $3d$, $4s$, and $4p$ for both Co and Cu atoms; the inner core orbitals were considered frozen. The valence orbitals were explicitly made orthogonal to the core orbitals in the first iteration. In calculating the matrix elements of the Hamiltonian operator, the greatest difficulty is posed by the Coulomb electron–electron repulsion term. To render this term tractable, a model electron density is constructed by least-squares fitting the ''real'' charge density to a multicenter multipolar expansion.[34] In the present calculation all terms with $l=0$ in the expansion were included; higher terms were not considered necessary due to the approximately spherical charge distribution in metallic systems.

We have considered clusters of 79 atoms with octahedral symmetry, namely, Co_NCu_{79-N} ($N=1,13,19,43,55$), consisting of a central Co atom coordinated to varying numbers of shells of Co atoms, and outer shells consisting of Cu atoms, in the fcc structure. Unless otherwise stated, the lattice parameter of fcc Cu was used in the calculations. These clusters were embedded in the potential field generated by the electron density and the nuclei of approximately 1500 Cu atoms to represent the host. The electron density of the atoms of the embedding was obtained by atomic DFT calculations.[27]

To study the magnetic properties, we calculated the local spin magnetic moment at each atomic site, integrating the spin density within a Wigner–Seitz cell. For all clusters, ferromagnetic coupling was assumed among the Co atoms. We also calculated the contributions to the magnetic hyperfine field at the Co nuclei. The Fermi or contact contribution to the hyperfine field can be determined by the spin density at the nuclear positions through the expression:[35]

$$B_C=\frac{8}{3}\pi\mu_B[\rho_\uparrow(0)-\rho_\downarrow(0)], \tag{3}$$

where μ_B is the Bohr magneton. Only the valence contribution is obtained from the cluster calculations; the core contribution ($1s$-$3s$) is obtained from DFT atomic calculations, for the electronic configuration of the atom as in the cluster. The dipolar contribution to the hyperfine field was calculated only at the Co atom sites at the boundary of the grains, where a non-negligible anisotropy of the spin density is expected, and is determined by the following expression:[35]

$$B^D_{ij}=\frac{1}{2}g_e\mu_B\int[\rho_\uparrow(\mathbf{r})-\rho_\downarrow(\mathbf{r})]\frac{(3x_ix_j-\delta_{ij}r^2)}{r^5}d^3r, \tag{4}$$

where B^D_{ij} are the components of the tensor of the dipolar hyperfine field and $x_i, x_j = x,y,z$.

Mulliken populations were employed to construct partial densities of states (PDOS).[27] The PDOS is obtained by broadening the cluster discrete energy levels by Lorentzians, with an appropriate half-width, and weighted by the Mulliken-type population of the atomic orbital considered.

III. RESULTS AND DISCUSSION

A. Local charges and magnetic moments

In Fig. 1 the $Co_{13}Cu_{66}$ cluster is depicted. The clusters with a larger number of Co atoms were constructed in a similar manner, substituting further shells of Cu atoms by Co, in the fcc structure. A shell is defined as a set of atoms at the same distance from the center. We employed the following notation: the central Co atom will be labeled Co0 and the consecutive shells with respect to the central atom will be

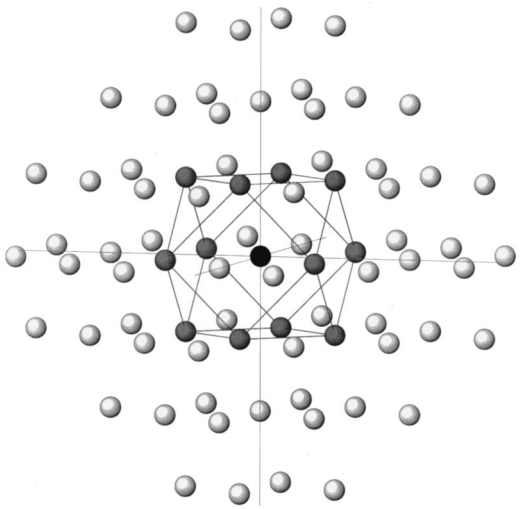

FIG. 1. Representation of the cluster $Co_{13}Cu_{66}$. Gray spheres are Co atoms at the interface (last shell) and the black sphere is the inner Co atom.

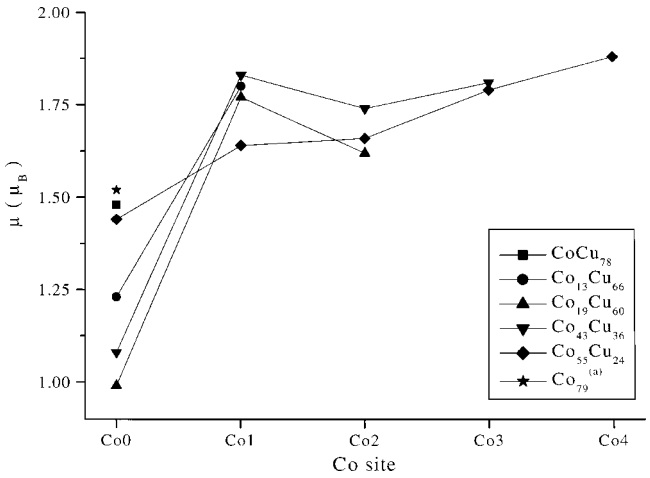

FIG. 2. Local magnetic moments for all cobalt sites for the clusters Co_NCu_{79-N} ($N=1$, 13, 19, 43, and 55) and for Co_{79}. Lines drawn are to guide the eye. (a) For lattice parameter of fcc Co ($a=3.54$ Å).

labeled Co1, Co2, Co3, and Co4 for the first, second, third, and fourth neighbors, respectively. Table I displays the ''environment'' of the Co atom sites, which helps us analyze the results. For ''environment'' we mean the number of Co and Cu atoms nearest neighbors to each Co atom site. For the Co3 and Co4 sites, the environment (12 atoms in fcc structure) is completed with copper atoms from the embedding (indicated by an asterisk), which are not included in the variational approach; therefore results obtained for these sites may not be as accurate as for the inner sites. For the sake of comparison, we have also made electronic structure calculations for a 79-atoms embedded cobalt cluster representing bulk fcc-Co (Co_{79}), with the lattice parameter of cobalt. In Fig. 2 are shown the calculated local magnetic moments (LMM) at the different cobalt sites for the clusters considered, obtained by integrating the spin density within a volume equal to the Wigner–Seitz cell pertaining to the site. The results for the Co grains of up to 43 atoms show an oscillatory behavior for the LMM, but with a tendency to increase from the center to the interface. In the grain with 55 cobalt atoms the LMM increases monotonically from the center to the interface. In the figure is also shown the LMM for Co_{79}, calculated at the central Co atom of the cluster, since the environment of this atom best represents that of bulk Co. The experimental value of the magnetic moment of fcc Co is $1.75\mu_B$.[36] The correction made in Ref. 37 to obtain only the spin contribution of the experimental magnetic moment (excluding the orbital contribution), using a g-factor of 2.17, resulted in a value of $1.61\mu_B$ for the spin component. Our calculated LMM for Co_{79} is $1.52\mu_B$ which is slightly smaller than the value obtained in Ref. 37. In Table II are tabulated the partial orbital contributions to the LMM of the same sites as in Fig. 2, but in this case these are obtained from the difference between the spin-up and spin-down Mulliken-type populations. This procedure results in total moments that may be slightly different from the LMM shown in Fig. 2. For the impurity of Co in Cu the result indicates the formation of a magnetic moment, which agrees with first-principles calculations using the Korringa–Kohn–Rostoker Green's function (KKRGF)[38,39] and RSLMTOASA[20] methods, albeit with a somewhat higher value. A previous calculation with the KKRGF method[40] resulted in that the impurity is nonmagnetic. Although the method used in Refs. 38, 39 and 40 is essentially the same, this disagreement in results is due to the fact that in the earlier work reported in Ref. 40 a ''single-site'' approximation for the self-consistent potential was employed. A calculation reported for a smaller cluster, employing a discrete variational method, resulted in a nonmagnetic impurity.[21] We believe that this discrepancy with our result is due to the smaller cluster size, as well as the less accurate model potential (SCC) employed in the calculation of Ref. 21.

TABLE I. Environment of the Co atom sites. The asterisk indicates copper atoms of the embedding.

Site	$CoCu_{78}$	$Co_{13}Cu_{66}$	$Co_{19}Cu_{60}$	$Co_{43}Cu_{36}$	$Co_{55}Cu_{24}$
Co0	12 Cu	12 Co	12 Co	12 Co	12 Co
Co1		5 Co, 7 Cu	7 Co, 5 Cu	11 Co, 1 Cu	12 Co
Co2			4 Co, 8 Cu	8 Co, 4 Cu	8 Co, 4 Cu
Co3				5 Co, 4 Cu, 3 Cu*	7 Co, 2 Cu, 3 Cu*
Co4					5 Co, 2 Cu, 5 Cu*

From Tables I and II it is observed that for Co atom sites with coordination of 12 cobalt atoms, the alignment of the $4s$ and $4p$ moments is antiparallel to the $3d$ moments. This type of alignment of the valence orbital moments is similarly found in bulk fcc cobalt, as is seen in Table II. For Co atom sites with an increasing number of Cu atoms as their first neighbors, the $4s$ and $4p$ moments altogether have a tendency to align parallel to the $3d$ moment. It can be seen from Tables I and II that Co atom sites with an environment with 5 or more Cu atoms as first neighbors have their total ($4s$

TABLE II. Partial contributions to the local magnetic moments (in μ_B).

Site		$CoCu_{78}$	$Co_{13}Cu_{66}$	$Co_{19}Cu_{60}$	$Co_{43}Cu_{36}$	$Co_{55}Cu_{24}$	Co_{79}[a]
Co0	$3d$	1.449	1.324	1.074	1.182	1.509	1.557
	$4s$	0.005	−0.033	−0.034	−0.028	−0.021	−0.017
	$4p$	0.018	−0.057	−0.054	−0.041	−0.036	−0.081
Co1	$3d$		1.822	1.795	1.869	1.716	
	$4s$		0.021	0.019	0.011	−0.004	
	$4p$		−0.006	−0.006	−0.036	−0.081	
Co2	$3d$			1.614	1.750	1.688	
	$4s$			0.006	−0.005	0.000	
	$4p$			0.005	−0.022	−0.015	
Co3	$3d$				1.801	1.811	
	$4s$				0.019	0.020	
	$4p$				0.024	−0.012	
Co4	$3d$					1.867	
	$4s$					0.030	
	$4p$					−0.009	

[a]For lattice parameter of fcc Co ($a=3.54$ Å).

$+4p$) moments aligned parallel to the $3d$ moments of Co. For all cluster sizes considered, the copper atoms at the interface have $3d$ moments coupled parallel to the Co-$3d$, and $4s$ and $4p$ moments coupled antiparallel. Although the values of the $4s$ and $4p$ moments change and thus may lead to an increase of the LMM at the Co atom sites in the direction of the grain boundaries, the contribution primarily responsible for the oscillatory behavior is from the $3d$ moments, as seen in Table II. For the grains, the value of the $3d$ moment at the Co0 site ranges from 1.07 to $1.51\mu_B$, at the Co1 site increases and ranges from 1.72 to $1.87\mu_B$, at the Co2 site slightly decreases and ranges from 1.61 to $1.75\mu_B$ and at the Co3 and Co4 sites the $3d$ moments increase again to 1.81 and $1.87\mu_B$, respectively. Similar results of oscillatory behavior with a tendency to increase the LMM at sites near and on the interface of the grains is obtained in Ref. 21. Different results are obtained in Ref. 20 with the RSLMTOASA method, the LMM increases at the inner sites of the grains. From Table II is also seen that the partial orbital contributions at the Co0 site for the $Co_{55}Cu_{24}$ and Co_{79} clusters are very similar. This demonstrates that, as the grains increase, the orbital contributions to the LMM of the inner atoms converge rapidly to the bulk values.

In Table III are presented the Mulliken populations (orbital electron occupancy) and net charges at the cobalt sites for all grains considered. It is seen that considerable charge transfer takes place. Larger positive charges are seen at site Co0 in all cases, mainly due to smaller $4s$ and $4p$ electron populations. The sign of the net charge oscillates from the central atoms to the interface sites; Co0 sites have positive charges, Co1 sites have negative charges, etc. This oscillatory behavior of the net charges is due to the variation of the population mainly of the $4s$ and $4p$ orbitals and in minor proportion to the population of the $3d$ orbitals. It is interesting to observe these Friedel-like oscillations in systems of small dimensionality.

At this point, it is worthwhile to further compare our results with those of Ref. 21 since a similar method was employed. As mentioned previously, differing from our results, in Ref. 21 it was found that the magnetism of the Co impurity in Cu is completely quenched. This discrepancy may be ascribed to a less accurate model potential utilized in Ref. 21 [self-consistent charge (SCC)], as well as the smaller cluster considered to represent the system ($CoCu_{42}$). For the Co clusters in Cu, the same tendency of increasing magnetic moments in the direction of the boundary as found here was obtained. However, generally higher values of the Co $3d$ moments were calculated particularly at the interface sites. For $Co_{43}Cu_{12}$, the calculated $3d$ moments of the Co2 and Co3 sites were 2.05 and $2.12\,\mu_B$, respectively, which may be compared to the present values 1.75 and $1.8\,\mu_B$ (see Table II). This difference may be due to the smaller cluster sizes in Ref. 21, with one shell less than ours to represent the Co/Cu systems, since truncation of the bonds will result in Co spin moments tending to the free atom value. In Ref. 21 calculated values of hyperfine fields are not reported, nor are spin-density maps presented.

B. Local density of states

In Fig. 3 is shown the local density of states (LDOS) of the valence bands for the Co0 and Co4 sites, and for the copper atoms at the interface, for the cluster $Co_{55}Cu_{24}$. We denominate ''interface'' the Co atoms of the last shell in the grain, although Co atoms in other shells may also be in contact with Cu atoms. It is observed that the majority-spin bands at the Co sites are almost filled and the minority-spin bands are partially filled, giving rise to magnetic moments. For the copper atom sites it is observed that both the majority and minority-spin bands are almost totally occupied. Since the spin-up bands of Co overlap considerably the Cu bands, one may expect considerable hybridization (which is not the

TABLE III. Mulliken populations and net charges at Cobalt sites. Net charge is defined as the atomic number Z minus total population on the atom.

Site		$CoCu_{78}$	$Co_{13}Cu_{66}$	$Co_{19}Cu_{60}$	$Co_{43}Cu_{36}$	$Co_{55}Cu_{24}$
Co0	3*d*	8.078	7.966	7.990	8.012	8.051
	4*s*	0.035	0.363	0.357	0.359	0.370
	4*p*	0.680	0.252	0.240	0.275	0.289
	Net charge	0.206	0.420	0.413	0.355	0.290
Co1	3*d*		7.842	7.870	7.852	7.956
	4*s*		0.710	0.715	0.710	0.523
	4*p*		0.602	0.499	0.545	0.539
	Net charge		−0.155	−0.084	−0.107	−0.018
Co2	3*d*			8.010	7.958	7.950
	4*s*			0.506	0.492	0.458
	4*p*			0.485	0.487	0.439
	Net charge			0.001	0.063	0.152
Co3	3*d*				7.914	7.919
	4*s*				0.602	0.701
	4*p*				0.463	0.531
	Net charge				0.021	−0.151
Co4	3*d*					7.911
	4*s*					0.642
	4*p*					0.273
	Net charge					0.173

case for Co spin-down). It is interesting to notice that for the interface site (Co4 for the cluster $Co_{55}Cu_{24}$), the Fermi level crosses the minority-spin DOS peak at its maximum; for the inner Co site the minority-spin DOS is wider and shows more structure. These same features are also obtained for $Co_{13}Cu_{66}$, $Co_{19}Cu_{60}$, and $Co_{43}Cu_{36}$. Figure 4 shows the LDOS for the central sites (Co0) for the Co impurity in Cu represented by Co_1Cu_{78} and for Co_{79} representing bulk Co. It is observed that the LDOS of the Co0 site for Co_{79} is quite similar to the LDOS of the Co0 site of the grain $Co_{55}Cu_{24}$ shown in Fig. 3; this is consistent with the similarity obtained in the calculated orbitals contributions to the LMM for

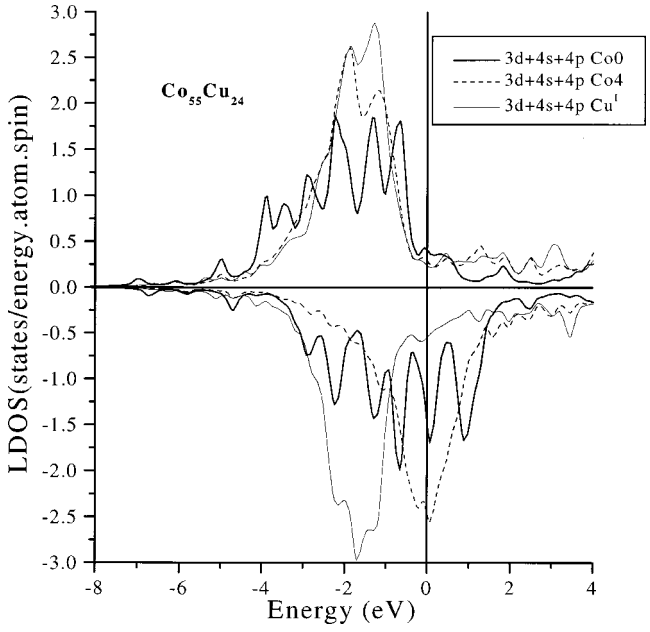

FIG. 3. LDOS for the cluster $Co_{55}Cu_{24}$ at the central (Co0) and interface (Co4) Co atoms sites, and at the interface Cu (Cu^I) atom site.

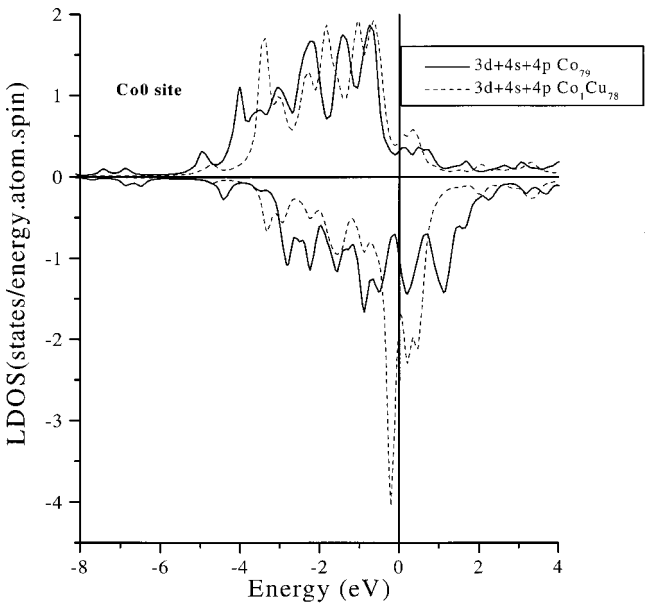

FIG. 4. LDOS for the cluster Co_{79} (representing bulk fcc Co) and Co_ICu_{78} at their central (Co0) sites.

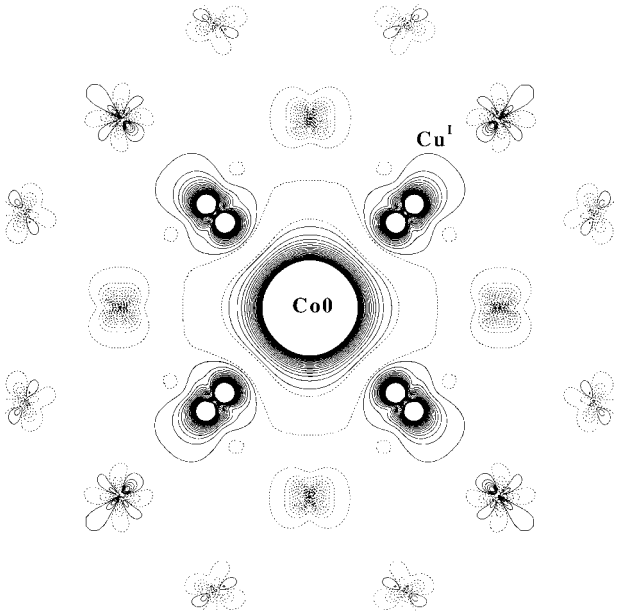

FIG. 5. Spin-density contours map of the cluster Co_ICu_{78} in a plane containing the central atom and four of its nearest neighbors. The Cu atoms nearest neighbors to the impurity are labeled Cu^I. Contours range from -0.0001 to $-0.01e/a_0^3$ with intervals $4.95\times10^{-4}e/a_0^3$, and from 0.0001 to $0.01e/a_0^3$, with intervals $4.95\times10^{-4}e/a_0^3$. Solid lines are positive values.

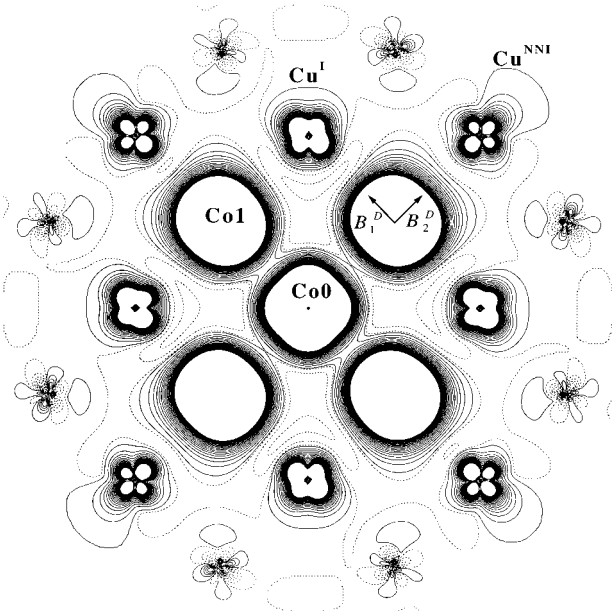

FIG. 6. Spin-density contours map of the cluster $Co_{13}Cu_{66}$ in a plane containing the central atom and four of its nearest neighbors. In one of the Co atoms at site Co1, the directions of the dipolar contributions B_1^D and B_2^D are indicated by arrows. The Cu atoms at the interface and nearest neighbors to the interface are labeled Cu^I and Cu^{NNI}, respectively. Contour specifications as in Fig. 5.

these central sites as remarked in Sec. III A. For the site of the impurity, it is observed that the minority-spin bands DOS present a narrow peak, which is crossed by the Fermi level almost at its maximum. This feature was also noticed for the interface sites of the grains; this indicates that the impurity behaves similarly to boundary sites, which may be understood considering that in both cases the Co–Co bonds are truncated.

C. Spin density contour maps

In Figs. 5–9 are shown the spin density contour maps for the clusters Co_1Cu_{78}, $Co_{13}Cu_{66}$, $Co_{19}Cu_{60}$, $Co_{43}Cu_{36}$, and $Co_{55}Cu_{24}$, respectively, in a plane containing the central atom (Co0) and four of the nearest neighbors (Co1). In Fig. 5 one can see the formation of the local spin moment of the Co impurity in the copper matrix. The copper atoms at the interface (Cu^I) are spin-polarized parallel to the Co ($3d$) orbitals with LMM $0.03\,\mu_B$ (as obtained by volume integration). In Fig. 6 it is clearly observed that there is significant anisotropy of the spin density in the environment of the atoms pertaining to the site Co1. In one of the atoms belonging to this site the direction of two of the components of the dipolar hyperfine field (see Sec. III D), in the system of principal axis, are indicated by the arrows. From Fig. 6 it is also observed that Cu^I atoms and copper atoms nearest neighbors to the interface (Cu^{NNI}) of the grain are spin-polarized parallel to the Co-$3d$ orbitals; their LMM is $0.04\,\mu_B$. The dashed lines between the Co0 and Co1 sites represent the negative contribution to the spin density mainly from the $4s$ and $4p$ orbitals of the central atom and of the copper atoms at the interface. In Fig. 7 it is observed that the Co1 and Co2 sites have smaller spin-density anisotropy as compared with the Co1 site in Fig. 6; the copper atoms at the interface (not seen in the figure) are spin-polarized parallel to the Co-$3d$ orbitals, with LMM $0.03\,\mu_B$. In Fig. 8 it is observed that the spin density at the Co2 site has even smaller anisotropy as compared to the Co1 site in Fig. 6. The Co3 site also has smaller anisotropy (not seen in the figure). Here it is ob-

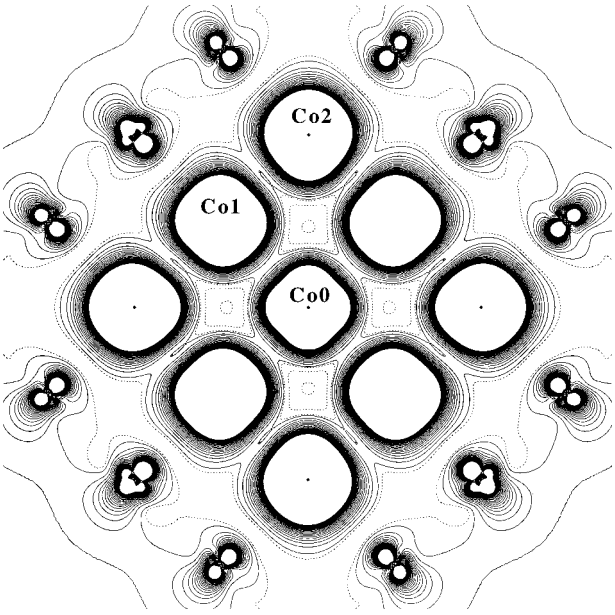

FIG. 7. Spin-density contours map of the cluster $Co_{19}Cu_{60}$ in a plane containing the central atom and four of its nearest neighbors. Contour specifications as in Fig. 5.

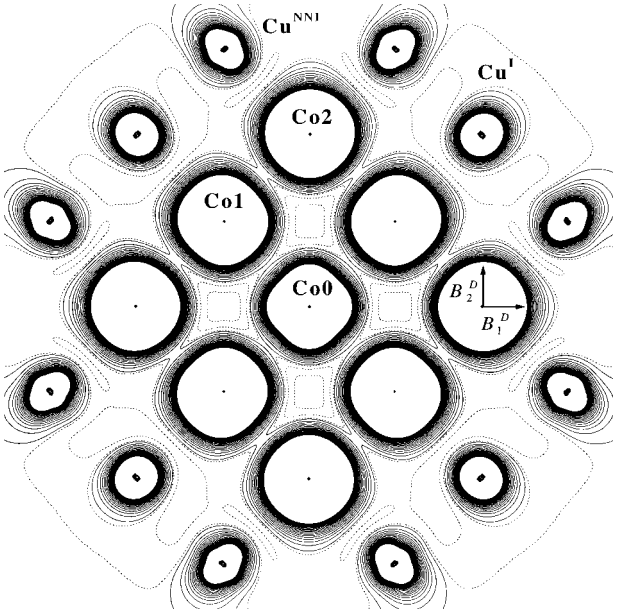

FIG. 8. Spin-density contours map of the cluster $Co_{43}Cu_{36}$ in a plane containing the central atom and four of its nearest neighbors. No Co3 sites are contained in this plane. In one of the Co atoms at site Co2, the directions of the dipolar contribution B_1^D and B_2^D are indicated by arrows. The Cu atoms at the interface and nearest neighbors to the interface are labeled Cu^{I} and Cu^{NNI}, respectively. Contour specifications as in Fig. 5.

served that Cu^{I} and Cu^{NNI} atoms have spin-polarization parallel to the Co-3d orbitals with LMM 0.07 and 0.05 μ_B, respectively. Finally, in Fig. 9 it is observed that the Co1 and Co2 sites have small spin-density anisotropy. The same is true for Co3 (this site not seen in the figure). For the interface site (Co4) a higher spin-density anisotropy is observed; Cu^{I} atoms have even higher spin polarization, parallel to the Co-3d orbitals, with a LMM of 0.08 μ_B. However, this increase in the local moments of Cu^{I} and Cu^{NNI} atoms for the largest grains ($Co_{43}Cu_{36}$ and $Co_{55}Cu_{24}$) could be partially due to spurious cluster surface effects, since for these the interface Cu atoms are at the surface of the total clusters. These figures will be very useful for interpreting the results of the calculated dipolar contribution to the hyperfine field in Sec. III D.

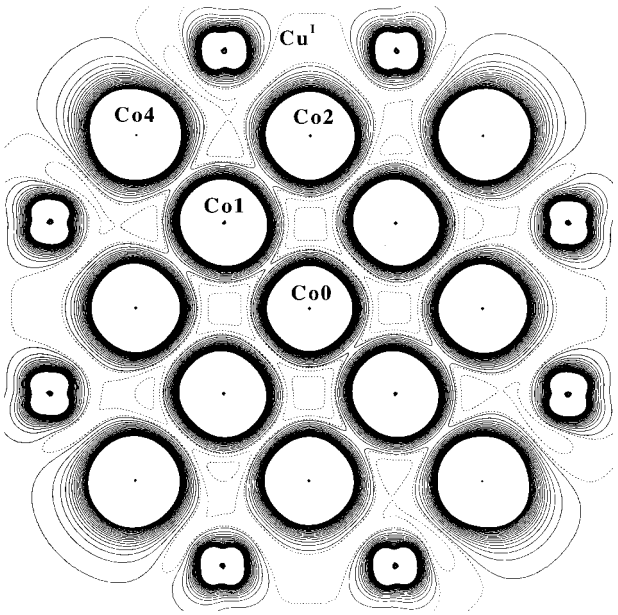

FIG. 9. Spin-density contours map of the cluster $Co_{55}Cu_{24}$ in a plane containing the central atom and four of its nearest neighbors. No Co3 sites are contained in this plane. The Cu atoms at the interface are labeled Cu^{I}. Contour specifications as in Fig. 5.

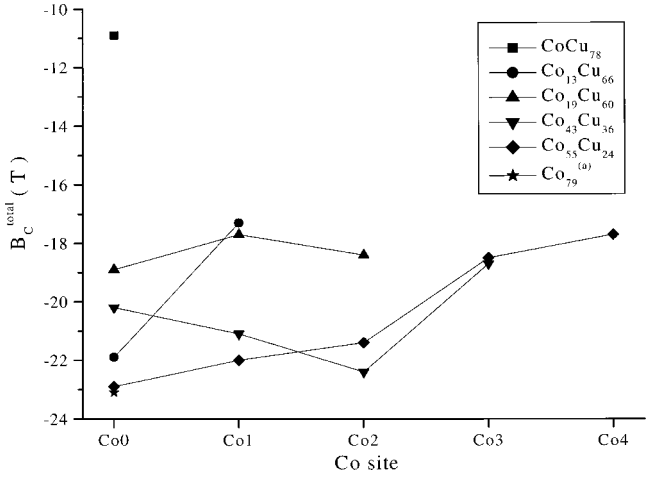

FIG. 10. Total contact hyperfine field for all cobalt sites for the clusters Co_NCu_{79-N} ($N=1$, 13, 19, 43, and 55) and for Co_{79}. Lines drawn are to guide to eye. (a) For lattice parameter of fcc Co ($a=3.54$ Å).

D. Contribution to the magnetic hyperfine field

In Fig. 10 is shown the calculated total contribution to the contact magnetic hyperfine field (HF) for Co atom sites for all the clusters considered. In the nonrelativistic approximation, only s electrons are found at the nuclear site. From the figure an oscillatory behavior of the magnitude of the contact HF for the grains is observed, but with a tendency to decrease in the direction of the interface. The exception is the cluster with 55 cobalt atoms, in which the magnitude of the contact HF decreases continuously from the center to the interface sites. The contact HF found for bulk fcc-Co is -23.1 T. The experimental value of the HF for bulk Co fcc is -21.5 T,[41] which is slightly smaller than our result, but sufficiently similar to give us confidence in the calculated values obtained for the grains. In Figs. 11 and 12 are shown the core and valence orbital contributions to the contact HF, respectively. The core contribution is due to the polarization of the 1s-3s shells by the 3d moment and is always negative. The main contribution to the contact HF comes from the core orbitals, and both the core and valence orbital contributions show oscillatory behavior. Here the $Co_{55}Cu_{24}$ cluster is also the exception, its valence orbital contributions to the contact HF increase continuously from negative to positive values. It is interesting to observe that from Figs. 2 and 11 a proportionality is inferred between the core orbitals contribution to the contact HF and the local magnetic moments.

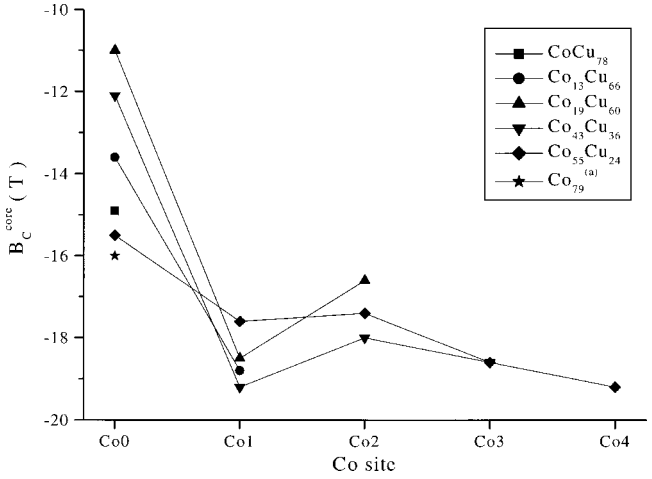

FIG. 11. Core contribution to the contact hyperfine field for all cobalt sites for the clusters Co_NCu_{79-N} ($N=1$, 13, 19, 43, and 55) and for Co_{79}. Lines drawn are to guide to eye. (a) For lattice parameter of fcc Co ($a=3.54$ Å).

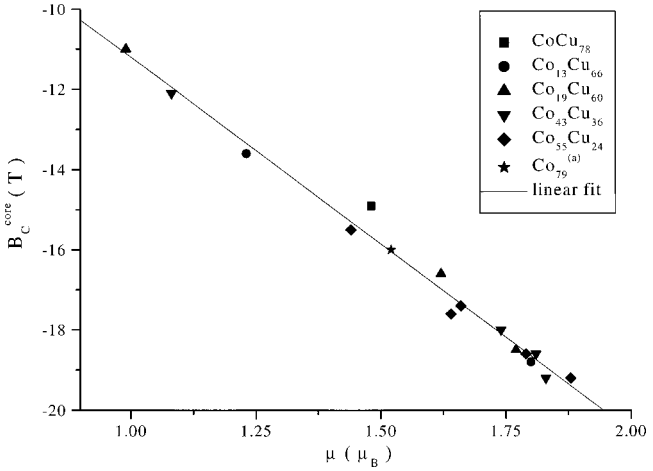

FIG. 13. Core contribution to the contact hyperfine field as a function of the local magnetic moment for the clusters Co_NCu_{79-N} ($N=1$, 13, 19, 43, and 55) and for Co_{79}.

The proportionality constant derived from the linear fit in Fig. 13 is $-9.3\,\mathrm{T}/\mu_B$, which is very similar to the value $-10\mathrm{T}/\mu_B$ reported previously.[20,42,43]

As mentioned previously, the LMM has a tendency to increase at sites near the interface; however, the magnitude of the total contact contribution to the HF has the opposite tendency. This is due to the following: it was inferred that the negative core orbital contribution to the HF is proportional to the LMM, therefore this contribution has larger negative values at sites near the interface. On the other hand, as seen in Fig. 12, the valence orbital contribution to the HF has larger negative values at inner sites, and smaller negative or positive values at sites near the interface, thus by summing these two contributions one obtains larger magnitudes to the total contact HF at inner sites. For the impurity, the value of the valence contribution is large and positive (4.1 T), this reduces the total contact HF to -10.9 T. From Figs. 11 and 12 it is also observed that the values of the core and valence contributions to the HF of $Co_{55}Cu_{24}$ and Co_{79} at the central site (Co0) are similar. In Ref. 20 the authors likewise report a continuous decrease of the magnitude of the HF from central to interface sites in clusters of up to 135 cobalt atoms in a copper host.

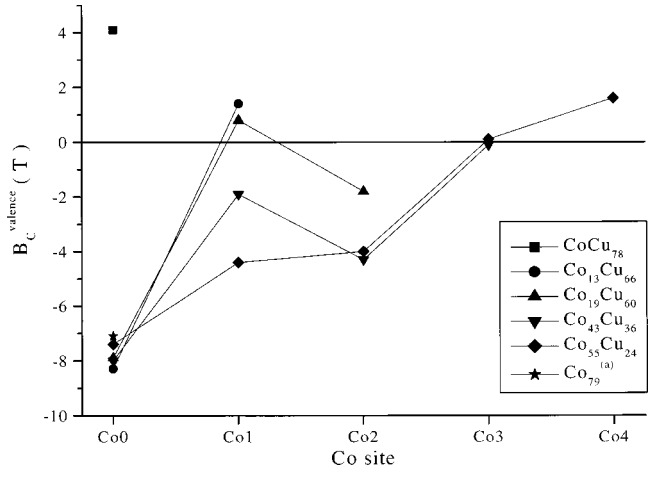

FIG. 12. Valence contribution to the contact hyperfine field for all cobalt sites for the clusters Co_NCu_{79-N} ($N=1$, 13, 19, 43, and 55) and for Co_{79}. Lines drawn are to guide to eye. (a) For lattice parameter of fcc Co ($a=3.54$ Å).

From Table II and Fig. 12 we may infer a correspondence between the sign of the $4s$ and $4p$ moments and the valence contributions to the contact HF. It is observed in Table II that at site Co0 for the clusters Co_NCu_{79-N}($N=13$,19,43,55) and for Co_{79} the values of the $4s$ moments are relatively large and negative; therefore this results in high negative values of the valence contributions to the HF, as shown in Fig. 12. The $4s$ moment of the impurity is positive and this results in a high positive value of the valence contribution to the HF. Going towards the interface sites, the $4s$ moments have a tendency to become aligned to the $3d$ moments, and this results in smaller negative or positive values of the valence contribution to the HF. For example, at the interface sites for the grains $Co_{13}Cu_{66}$ and $Co_{55}Cu_{24}$ (Co1 and Co4, respectively), we see large positive values for the $4s$ moments (and small negative values for the $4p$ moments) and this results in positive values of the valence contribution to the HF of 1.4 and 1.6 T, respectively.

NMR measurements on Co–Cu granular alloys prepared by the melt-spinning technique[12] show spectra with a distribution of HF values with two principal peaks. The highest peak has an average magnitude of the HF of 21.4 T, very near bulk fcc Co (21.6 T); the second peak is a distribution of HFs that range from 14.9 to 20 T. The first peak is attributed to the inner fcc Co atoms. The second peak is attributed to fcc Co_xCu_{1-x} alloys with $x=0.07-0.3$ formed near and at the interface of the grains. Other work, reported in Ref. 13, describes NMR measurements of Co grains in a Cu matrix, also prepared by melt-spinning. The authors found line frequencies corresponding to HFs of smaller magnitude than bulk fcc cobalt. Every narrow peak was attributed to a substitution of a nearest-neighbor Co atom by Cu, yielding a discrete decrease in the magnitude of the HF by a rate of

TABLE IV. Components in the system of principal axis of the dipolar contribution to the hyperfine field (in T)

Cluster	Site	B_1^D	B_2^D	B_3^D
$Co_{13}Cu_{66}$	Co1	+1.0	−4.2	+3.2
$Co_{19}Cu_{60}$	Co1	−1.4	+0.9	+0.5
	Co2	+2.3	−1.2	−1.1
$Co_{43}Cu_{36}$	Co2	−0.5	+0.3	+0.2
	Co3	−0.3	0.0	+0.3
$Co_{55}Cu_{24}$	Co2	−1.4	+0.8	+0.6
	Co3	−0.8	−0.9	+1.7
	Co4	−1.2	+3.6	−2.4

approximately −1.8 T per nearest-neighbor substitution. In spite of our clusters being smaller than in these experiments, the results we obtained agree in general with the tendency found in the NMR measurements, in that Co atoms with a larger number of Cu neighbors (such as occurs at the grain interface) have HFs of smaller magnitude.

Besides the contact contribution to the HF considered at all sites, we have also taken into account the dipolar contribution. This term gives an estimate of the anisotropy of the spin density around the atom for which it is calculated. For the calculation of this contribution, we considered the following sites: Co1 site in $Co_{13}Cu_{66}$, Co1 and Co2 sites in $Co_{19}Cu_{60}$, Co2 and Co3 sites in $Co_{43}Cu_{36}$, and Co2, Co3, and Co4 sites in $Co_{55}Cu_{24}$. These sites have been considered because they have environments with four or a greater number of copper atoms and thus non-negligible anisotropy in the spin density is expected, as explained in Sec. II. The results are tabulated in Table IV and have much smaller magnitudes than the contact HF, although still significant. The components of the dipolar contributions are given in the system of principal axis. The orientation of the principal axis is different for atoms of the same shell, but the components of the dipolar contributions to the HF are the same, since the atoms are equivalent by symmetry. For example, let us analyze the Co1 site of the cluster $Co_{13}Cu_{66}$ with the help of Fig. 6 and Table IV. We calculated the dipolar contribution at the atom indicated by the components B_1^D and B_2^D. From Table IV it is observed that the component with the largest magnitude is $B_2^D = -4.2$ T, i.e., the spin density anisotropy is larger in this direction (as visualized in Fig. 6) and thus the HF is enhanced in this direction. In Fig. 14 is shown the spin-density contours map of the $Co_{13}Cu_{66}$ cluster in a plane perpendicular to that of Fig. 6 containing the component B_2^D. This plane contains component B_3^D with a value +3.2 T, as well as B_2^D. It is seen that the spin-density anisotropy in the direction of B_2^D is larger than that in the direction of B_3^D; this is consistent with the result tabulated in Table IV. The smallest dipolar contributions have been obtained for cluster $Co_{43}Cu_{36}$ at the Co2 and Co3 sites, with magnitudes 0.5 and 0.3 T for their principal components, respectively.

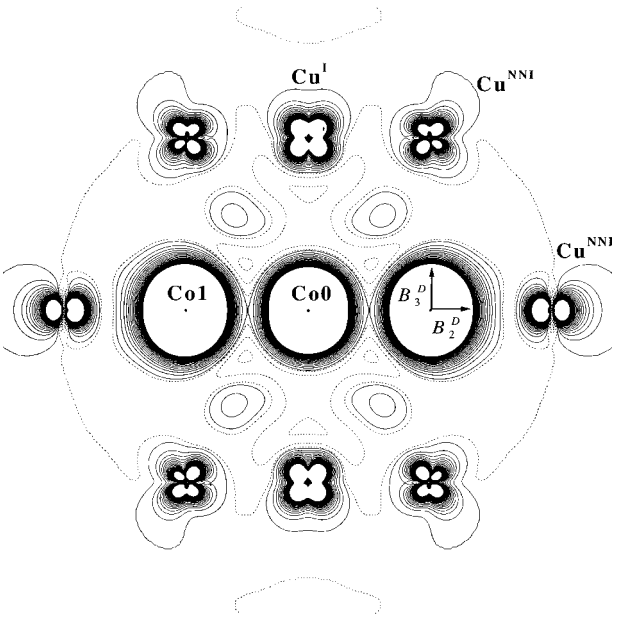

FIG. 14. Spin-density contours map of the cluster $Co_{13}Cu_{66}$ in a perpendicular plane to that of Fig. 6, containing the dipolar component B_2^D. The arrow marked B_3^D indicates the third component of the dipolar contribution in one of the Co atoms at site Co1. The Cu atoms at the interface and nearest neighbors to the interface are labeled Cu^I and Cu^{NNI}, respectively. Contour specifications as in Fig. 5.

IV. CONCLUSIONS

Electronic structure calculations have been performed for embedded clusters representing grains of up to 55 Co atoms in a Cu matrix. Our results indicate that the LMM at the Co atom sites for grains with up to 43 atoms show oscillatory behavior, with a tendency to increase from the center to the interface sites. The LMM for the cluster with 55 Co atoms increases continuously.

The magnitude of the total contact HF also shows oscillatory behavior but with a tendency to decrease towards the interface sites, for grains of up to 43 Co atoms. For the grain with 55 Co atoms, the magnitude of the contact HF decreases continuously from the center to the interface site. This behavior is explained by analyzing the contributions of the 4*s* electrons and is consistent with experimental observations obtained with ^{59}Co NMR spectroscopy.[12,13]

There exists a non-negligible dipolar contribution to the HF for Co atom sites near and at the interface of the grains. The largest magnitude of the dipolar contribution to the HF was found for the $Co_{13}Cu_{66}$ cluster, with −4.2 T for the main component.

ACKNOWLEDGMENTS

Calculations were performed partially in the Cray J90 of the Supercomputing Center of the Universidade Federal do Rio Grande do Sul. This work was supported by CNPq.

*Electronic address: diana@cat.cbpf.br

[1] A. E. Berkowitz, J. R. Mitchell, M. J. Carey, A. P. Young, S. Zhang, F. E. Spada, F. T. Parker, A. Hutten, and G. Thomas, Phys. Rev. Lett. **68**, 3745 (1992).
[2] J. Q. Xiao, J. S. Jiang, and C. G. Chien, Phys. Rev. Lett. **68**, 3749 (1992).
[3] P. Allia, C. Beatrice, M. Knobel, P. Tiberto, and F. Vinai, J. Appl. Phys. **76**, 6817 (1994).
[4] H. Sato, K. Honda, Y. Aoki, N. Kataoka, I. J. Kim, and K. Fukamichi, J. Magn. Magn. Mater. **152**, 109 (1996).
[5] M. Tsunoda, K. Okuyama, M. Ooba, and M. Takahashi, J. Appl. Phys. **83**, 7004 (1998).
[6] Y. Ueda, S. Ikeda, and S. Chicazawa, Jpn. J. Appl. Phys., Part 1 **35**, 3414 (1999).
[7] A. N. Pohorilyi, A. F. Kravetz, O. V. Shypil, A. Ya. Vovk, C. S. Kim, and H. R. Khan, J. Magn. Magn. Mater. **196–197**, 43 (1999).
[8] P. Allia, P. Tiberto, F. Vinai, L. Pareti, and G. Turilli, J. Magn. Magn. Mater. **196–197**, 56 (1999); P. Allia, P. Tiberto, and F. Vinai, *ibid.* **203**, 76 (1999).
[9] M. Kuzminski, A. Slawska-Waniewska, and H. K. Lachowicz, IEEE Trans. Magn. **35**, 2853 (1999); M. Kuzminski, A. Slawska-Waniewska, H. K. Lachowicz, and M. Knobel, J. Magn. Magn. Mater. **205**, 7 (1999).
[10] L. Xing and Y. C. Chang, Phys. Rev. B **48**, 4156 (1993); L. Xing, Y. C. Chang, M. B. Salomon, D. M. Frenkel, J. Shi, and J. P. Lu, *ibid.* **48**, 6728 (1993).
[11] M. A. Uimin, A. Ye. Yermakov, V. V. Serikov, A. Yu. Korobeinikov, and A. K. Shtolz, Phys. Status Solidi A **165**, 337 (1998).
[12] M. Malinowska, M. Wójcik, S. Nadolski, E. Jedryka, C. Mény, P. Panissod, M. Knobell, A. D. C. Viegas, and J. E. Schmidt, J. Magn. Magn. Mater. **198–199**, 599 (1999).
[13] E. H. C. P. Sinnecker, I. S. Oliveira, P. Tiberto, and A. P. Guimarães, J. Magn. Magn. Mater. **218**, L132 (2000).
[14] J. Stöhr and R. Nakajima, J. Phys. IV **(C2)**, 47 (1997); J. Stöhr, J. Magn. Magn. Mater. **200**, 470 (1999).
[15] M. G. Samant, J. Stöhr, S. S. P. Parkin, G. A. Held, B. D. Hermsmeier, F. Herman, M. van Schilfgaarde, L. C. Duda, D. C. Mancini, N. Wassdalh, and R. Nakajima, Phys. Rev. Lett. **72**, 1112 (1994).
[16] J. Hunter Dunn, D. Arvanitis, N. Martensson, M. Tisher, F. May, M. Russo, and K. Baberschke, J. Phys.: Condens. Matter **7**, 1111 (1995).
[17] M. Tisher, O. Hjortstam, D. Arvanitis, J. Hunter Dunn, F. May, K. Baberschke, J. Trygg, J. M. Wills, B. Johansson, and O. Eriksson, Phys. Rev. Lett. **75**, 1602 (1995).
[18] P. Srivastava, F. Wilhelm, A. Ney, M. Farle, H. Wende, N. Haack, G. Ceballos, and K. Baberschke, Phys. Rev. B **58**, 5701 (1998).
[19] D. A. Eastham, Y. Qiang, T. H. Maddock, J. Kraft, J.-P. Schille, G. S. Thompson, and H. Haberland, J. Phys.: Condens. Matter **9**, L497 (1997).
[20] R. N. Nogueira, Ph.D. thesis, Instituto de Física, Universidade de São Paulo; R. N. Nogueira and H. M. Petrilli, Phys. Rev. B (to be published).
[21] X. Chuanyun, Y. Jinlong, D. Kaiming, and W. Kelin, Phys. Rev. B **55**, 3677 (1997).
[22] Z.-Q. Li and B.-L. Gu, Phys. Rev. B **47**, 13 611 (1993).
[23] K. Miúra, H. Kimura, and S. Imanaga, Phys. Rev. B **50**, 10 335 (1994).
[24] N. Fujima and Sh. Sakurai, J. Phys. Soc. Jpn. **68**, 586 (1999).
[25] D. E. Ellis, Int. J. Quantum Chem. **2S**, 35 (1968).
[26] D. E. Ellis and G. S. Painter, Phys. Rev. B **2**, 2887 (1970).
[27] D. E. Ellis and D. Guenzburger, Adv. Quantum Chem. **34**, 51 (1999).
[28] R. G. Parr and W. Yang, *Density Functional Theory of Atoms and Molecules* (Oxford University, New York, 1989).
[29] S. H. Vosko, L. Wilk, and M. Nusair, Can. J. Phys. **58**, 1200 (1980).
[30] D. M. Ceperley and B. J. Alder, Phys. Rev. Lett. **45**, 566 (1980); D. Ceperley, Phys. Rev. B **18**, 3126 (1978).
[31] C. B. Haselgrove, Math. Comput. **15**, 323 (1961).
[32] H. Conroy, J. Chem. Phys. **47**, 5307 (1967).
[33] R. S. Mulliken, J. Chem. Phys. **23**, 1833 (1955); **23**, 1841 (1955).
[34] B. Delley and D. E. Ellis, J. Chem. Phys. **76**, 1949 (1982).
[35] A. Abragam, *The Principles of Nuclear Magnetism* (Oxford University, Oxford, 1961).
[36] J. Crangle, Philos. Mag. **46**, 499 (1955).
[37] V. L. Moruzzi, P. M. Marcus, K. Schwarz, and P. Mohn, J. Magn. Magn. Mater. **54–57**, 955 (1986).
[38] B. J. Braspenning, R. Zeller, A. Loddler, and P. H. Dederichs, Phys. Rev. B **29**, 703 (1984).
[39] B. Dritler, H. Ebert, R. Zeller, and P. H. Dederichs, Phys. Rev. B **39**, 6334 (1989).
[40] R. Podloucky, R. Zeller, and P. H. Dederichs, Phys. Rev. B **22**, 5777 (1980).
[41] A. M. Portis and A. C. Gossard, J. Appl. Phys. **31**, 205S (1960).
[42] R. N. Nogueira and H. M. Petrilli, Phys. Rev. B **53**, 15 071 (1996).
[43] R. N. Nogueira and H. M. Petrilli, Hyperfine Interact. **120/121**, 131 (1999).